Fragmentation of Interstellar Methanol By Collisions With $He^{\cdot+}$: an Experimental and Computational Study: Electronic Supplementary Information (ESI)

Vincent Richardson[a], Emília Valença Ferreira de Aragão [b,c], Xiao He[a], Fernando Pirani[b,d], Luca Mancini[b], Noelia Faginas-Lago[b,c], Marzio Rosi[d], Luca Matteo Martini[a] and Daniela Ascenzi[a,*]

[a] *Department of Physics, University of Trento, Trento, Italy.*
[b] *Department of Chemistry, Biology and Biotechnology, Universitá degli studi di Perugia, Perugia, Italy.*
[c] *Master-Tec s.r.l., Via Sicilia 41, Perugia, Italy.*
[d] *Department of Civil and Environmental Engineering, Universitá degli studi di Perugia, Perugia, Italy.*
∗ *correspondig author, e-mail: daniela.ascenzi@unitn.it*

1 Mass spectrum of reaction products

A typical mass spectrum obtained for the products of the reaction between $He^{\cdot+}$ and methanol (CH_3OH) is shown in Fig. 1. The mass spectrum is the average of four scans taken at a collision energy E_{CM}=0.29 eV, using a 10% mixture of CH_3OH in Ar at an average pressure in the scattering cell (as read by the spinning rotor gauge) of 5.0x10^{-5} mbar.

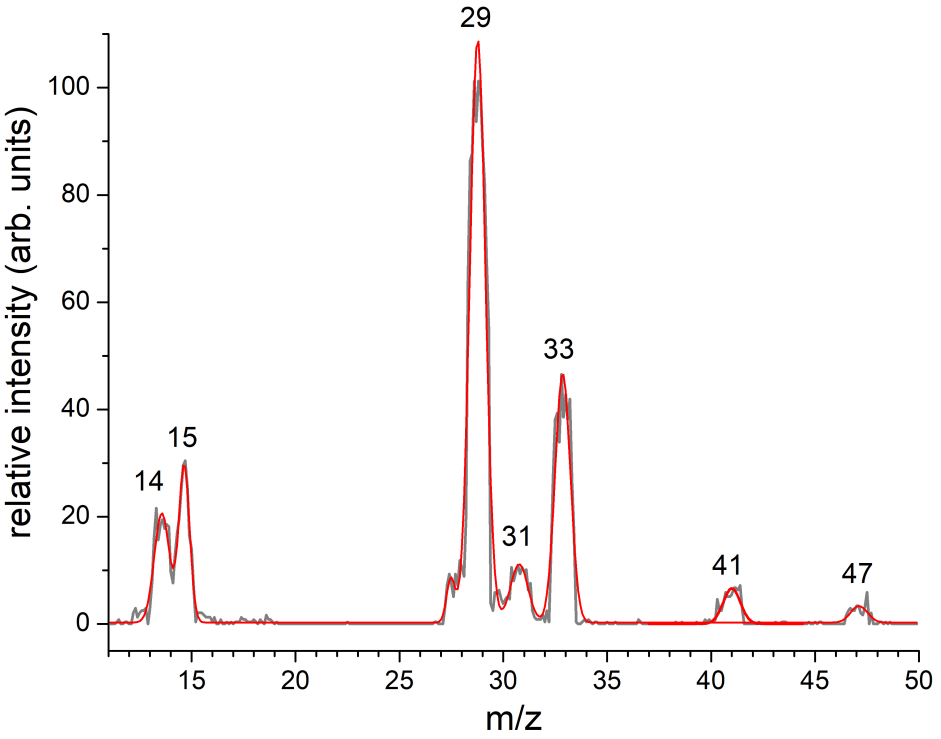

Figure 1: A representative mass spectrum from the reaction of $He^{\cdot+}$ with CH_3OH: grey line is the experimental data and red lines are best fits of the peaks using gaussian functions.

2 Determination of Effective Reaction Cell Length

The raw output from the experimental apparatus used in this work is in the form of ion counts and, in order to convert these into absolute reaction cross sections (σ), we make use of the Beer-Lambert Law.

Although the Beer-Lambert Law describes the absorption of light by a sample, the reaction of ions passing through a neutral can be considered in a similar way. The number of ions that pass through a cell without reacting is therefore given by the following expression:

$$I_0 = I_R \cdot exp(-\rho \cdot \sigma_{coll} \cdot l) \tag{1}$$

Where I_0 is the unreacted ion signal, I_R is the reagent ion signal, σ_{coll} is the collision CS, ρ is the density of the neutral gas and l is the length of the reaction cell. In this way, the number of ions undergoing reaction,

I_P, can be expressed as:

$$I_P = I_R.[1 - exp(-\rho \cdot \sigma_{rxn} \cdot l)] \tag{2}$$

Where σ_{rxn} is the CS of the reaction. Under the *thin target limit*, where reaction probabilities are small (i.e. $\rho\sigma_{rxn}l \ll 1$), this can be simplified as:

$$I_P = I_R.(\rho \cdot \sigma_{rxn} \cdot l) \tag{3}$$

ρ, the density of the neutral gas, in particles·cm^{-3}, is directly related to the pressure via the *Ideal Gas Law*:

$$\rho = \frac{P \cdot N_A}{R \cdot T} \tag{4}$$

Where N_A is Avogadro's Number, R is the gas constant in mbar·cm^3·K^{-1}·mol^{-1}, T is the temperature in K and P is the pressure in mbar. This means that if T and l are known, the reaction cross section (σ_{rxn}) can be determined by measuring the ion intensities as a function of the pressure. Alternatively, by simultaneously measuring I_R, I_P, T and P with a known l we are able to calculate reaction cross sections on a point-by-point basis.

The effective reaction cell length is therefore determined through comparison with literature data, using a re-phrasing of equation (3).

$$\frac{I_P}{I_R} = l \cdot \rho \cdot \sigma_{rxn} \tag{5}$$

By using a literature value of σ_{rxn} at a known temperature, we are therefore able to obtain a value for l by measuring $\frac{I_P}{I_R}$ as a function of the pressure.

As the effective reaction cell length depends on the trapping efficiency of the parent ion, in order to determine the effective reaction cell length for $He^{\cdot+}$, we have used the previously-studied reaction of $He^{\cdot+}$ with $SiCl_4$ [Fisher and Armentrout(1991)], the reaction pathways for which are given by Eqs. (6)-(10).

$$\mathrm{He}^{\bullet+} + \mathrm{SiCl_4} \rightarrow \mathrm{SiCl_4}^{\bullet+} + \mathrm{He} \quad (6)$$

$$\rightarrow \mathrm{SiCl_3}^{+} + \mathrm{Cl}^{\bullet} + \mathrm{He} \quad (7)$$

$$\rightarrow \mathrm{SiCl_2}^{\bullet+} + [\mathrm{Cl_2}] + \mathrm{He} \quad (8)$$

$$\rightarrow \mathrm{SiCl}^{+} + [\mathrm{Cl_3}]^{\bullet} + \mathrm{He} \quad (9)$$

$$\rightarrow \mathrm{Si}^{\bullet+} + [\mathrm{Cl_4}] + \mathrm{He} \quad (10)$$

The corresponding thermochemistries are given in Table 1.

Table 1: Reaction thermochemistries for the identified products of the reaction of $He^{\cdot+}$ with silicon tetrachloride ($SiCl_4$).

Reaction Products	**Eq.**	**Reaction Enthalpy (eV)**
$SiCl_4^{\cdot+}$ + He	**(6)**	-12.73 ± 0.07
$SiCl_3^{+}$ + $Cl^{\cdot}$ + He	**(7)**	-12.04 ± 0.14
$SiCl_2^{\cdot+}$ + Cl_2 + He	**(8)**	-9.44 ± 0.18
$SiCl^{+}$ + $Cl^{\cdot}$ + Cl_2 + He	**(9)**	-7.35 ± 0.40
$Si^{\cdot+}$ + $2Cl_2$ + He	**(10)**	-4.84 ± 0.05

IE(He) = 24.59 is taken from NIST
[Kramida *et al.*(2020)Kramida, Ralchenko, and Reader], while formation enthalpies for $SiCl_4$, $Cl^{\cdot}$ and $SiCl_x^{+}$ are taken from Fisher and Armentrout [Fisher and Armentrout(1991)].

The choice of $SiCl_4$ as calibrant for the reactions of $He^{\cdot+}$ ions is motivated by several factors:

i) existing literature values [Fisher and Armentrout(1991)] have been measured using a guided ion beam set-up very similar to the one used in the present experiments;

ii) the $He^{\cdot+}$-$SiCl_4$ and $He^{\cdot+}$-CH_3OH systems have similar reaction thermochemistries (compare Table 1 above with Table 1 in the main paper) which are the major factors affecting the product collection efficiency in guided ion beam experiments. In particular, large exothermicities lead to product ions having large velocities, therefore requiring large values of the octupole effective potential to be efficiently trapped (in the direction perpendicular to the octupole axis) and transferred to the quadrupole mass analyzer;

iii) the two systems are similar in the dynamics of the dissociative charge exchange, with the recombination energy of $He^{\cdot+}$ correlating

with a core excitation of $SiCl_4$, with the electron being removed from a $3s$ core orbital mostly localized on the chlorine atoms.

For the calibration of the Trento GIB-MS, we have focused on the major product channel given by Eq. (7), with the results of a series of scans of $\frac{I_P}{I_R}$ as a function of the neutral gas density for this process being shown in Fig. 2. From this, we have extracted an effective reaction cell length of 8.26 cm, with the $\pm 50\%$ error margin being a result of the uncertainty in literature CSs [Fisher and Armentrout(1991)].

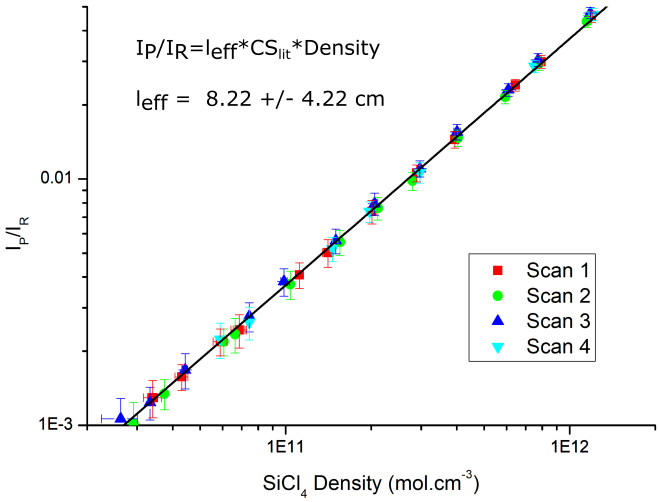

Figure 2: Product:Parent ion ratio as a function of neutral gas density for the m/z 63 product of the reaction of $He^{\cdot +}$ with silicon tetrachloride ($SiCl_4$).

3 Calibration of Absolute Cross Section Scale

In order to convert the relative cross sections measured as a function of E_{CM} into absolute cross sections, we have used the inverse procedure used to determine the effective cell length to determine the absolute cross section at a series of specific collision energies.

To do this, we have measured the intensities as a function of the CH_3OH pressure of the parent, the major m/z 29 product and the secondary products at m/z 33 and 47 products, with I_P being the sum of the three channels. From this, we are able to determine the absolute cross section using Eq. (5).

4 Potential Energy Surface for the dissociation process

In Figure 3 we report the schematic representation of the PES for the dissociation of the CH3OH$^+$ cation from its ground electronic state, calculated from optimized geometries using DFT theory and the B3LYP functional (CCSD(T)/aug-cc-pVTZ//B3LYP/aug-cc-pVTZ level of theory). Results can be compared with Fig. 6 in the main paper, where the functional ωB97X-D which includes dispersion is used. Since no significative differences are found in the optimized geometries the energies calculated at the Couple Cluster level are practically the same.

In Table 2 a comparison of the relative energies at DFT and CCSD(T) level of theory is presented with and without dispersion for all the stationary points of the PES. As expected, the energies calculated at the DFT and CCSD(T) level present some differences.

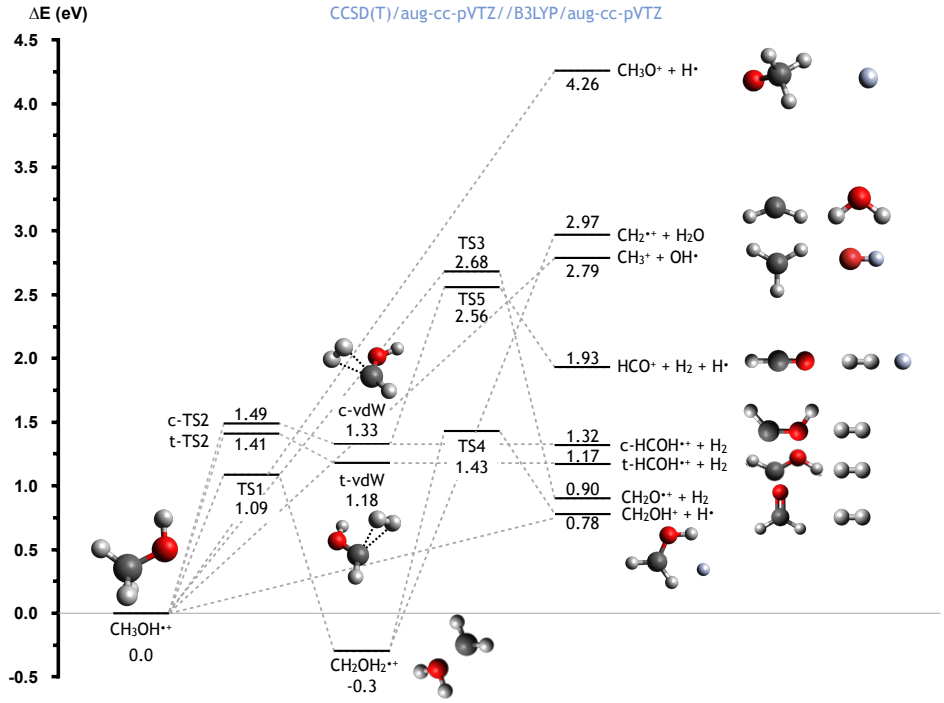

Figure 3: Schematic representation of the PES for the dissociation of the $CH_3OH^{\cdot+}$ cation, with the energies (reported in eV) evaluated at the CCSD(T)/aug-cc-pVTZ//B3LYP/aug-cc-pVTZ level of theory.

Table 2: List of electronic and zero-point correction energies of every chemical species present in the PES (see Fig. 6). The reported values correspond to geometries optimized at B3LYP/aug-cc-pVTZ and ωB97X-D/aug-cc-pVTZ levels. Single-point energies calculated at CCSD(T)/aug-cc-pVTZ are also reported.

Species	$\mathbf{E}_{B3LYP}$	$\mathbf{ZPE}_{B3LYP}$	$\mathbf{E}_{CCSD(T)}$	$\mathbf{E}_{\omega B97X-D}$	$\mathbf{ZPE}_{\omega B97X-D}$	$\mathbf{E}_{CCSD(T)}$
Reactants						
$CH_3OH^{\cdot+}$	-115.3834802290	0.046862	-115.1610651500	-115.3427669800	0.047375	-115.1608861500
Intermediates						
$CH_2OH_2^{+}$	-115.3877088790	0.049141	-115.1744274900	-115.3487310470	0.049888	-115.1743807800
c-vdW	-115.3221728350	0.038616	-115.1038208900	-115.2802537740	0.039612	-115.1041148800
t-wdW	-115.3276376270	0.039159	-115.1101419800	-115.2857365480	0.040158	-115.1103487900
Saddle Points						
TS1	-115.3341830470	0.044706	-115.1187243300	-115.2951345350	0.045424	-115.1185513800
c-TS2	-115.3209387610	0.039083	-115.0984926500	-115.2783404040	0.040486	-115.0988221400
t-TS2	-115.3243101610	0.040142	-115.1025841800	-115.2820869090	0.041269	-115.1027935800
TS3	-115.2752472980	0.041772	-115.0571624700	-115.2350888120	0.042414	-115.0570001700
TS4	-115.3265257360	0.042088	-115.1036224700	-115.2789373450	0.042714	-115.1028820700
TS5	-115.2700967010	0.029239	-115.0493468700	-115.2192954290	0.030206	-115.0485024500
Products						
$H^{\cdot}$	-0.5022596758	0.000000	-0.4998211760	-0.5028030558	0.000000	-0.4998211760
H_2	-1.1800238369	0.010064	-1.1726355789	-1.1766497389	0.010099	-1.1726355789
$CH_2^{\cdot+}$	-38.7864995920	0.016201	-38.6999427600	-38.7710525029	0.016326	-38.6999526950
CH_3^{+}	-39.4953916231	0.031189	-39.4057119600	-39.4806369666	0.031334	-39.4057120470
$OH^{\cdot}$	-75.7685991556	0.008428	-75.6455836420	-75.7407518340	0.008614	-75.6455765760
H_2O	-76.4661964901	0.021231	-76.3423029730	-76.4399218158	0.021641	-76.3422864420
HCO^{+}	-113.5928079680	0.016412	-113.3971405900	-113.5550634790	0.016551	-113.3969631700
c-$HCOH^{\cdot+}$	-114.1369264150	0.025246	-113.9283327900	-114.0978320400	0.025750	-113.9283170400
t-$HCOH^{\cdot+}$	-114.1424674090	0.025741	-113.9343018200	-114.1033368310	0.026186	-113.9342427300
$CH_2O^{\cdot+}$	-114.1526232090	0.023830	-113.9423733000	-114.1123021170	0.024165	-113.9423143700
CH_3O^{+}	-114.7109492640	0.033026	-114.4908106000	-114.6694558310	0.033561	-114.4907754800
CH_2OH^{+}	-114.8345316640	0.040416	-114.6260923400	-114.7967185830	0.040884	-114.6259744100

References

[Fisher and Armentrout(1991)] E. R. Fisher and P. Armentrout, *The Journal of Physical Chemistry*, 1991, **95**, 4765–4772.

[Kramida *et al.*(2020)Kramida, Ralchenko, and Reader] A. Kramida, Y. Ralchenko and J. Reader, *NIST Atomic Spectra Database (version 5.8)*, [Online], 2020.